



## Research article

# A chromogenic diarylethene-based probe for the detection of $\text{Cu}^{2+}$ in aqueous medium in *Drosophila* for early diagnosis of Alzheimer

Gautam Kumar<sup>a</sup>, Ananya Srivastava<sup>a</sup>, Prabhat Kumar<sup>b</sup>, S. Srikrishna<sup>b</sup>, Vinod P. Singh<sup>a,\*</sup>

<sup>a</sup> Department of Chemistry, Institute of Science, Banaras Hindu University, Varanasi, India

<sup>b</sup> Department of Bio Chemistry, Institute of Science, Banaras Hindu University, Varanasi, India

## ARTICLE INFO

## Keywords:

Colorimetric probe  
Copper(II) sensing  
Bioimaging  
Alzheimer's disease  
*Drosophila*

## ABSTRACT

A diarylethene-based probe (*Z*)-*N*'-(2-amino-5-chlorophenyl)(phenyl)methylene)-2-hydroxy benzohydrazide (**KBH**) has been proficiently developed and its structure has been confirmed by single crystal X-ray diffraction technique. It displays a selective and sensitive colorimetric sensing of  $\text{Cu}^{2+}$  ions in aqueous medium with a naked eye colour change from colourless to yellow. It exhibits a significantly low limit of detection as 1.5 nM. A plausible binding mechanism has been proposed using Job's plot, FT-IR, <sup>1</sup>H NMR titration, HRMS and DFT studies. The chemosensor is effectively reversible and reusable with EDTA. Test strip kit and real water sample analysis have been shown to establish its practical applicability. Further, the potential of **KBH** for the early diagnosis of  $\text{Cu}^{2+}$  ion-induced amyloid toxicity has been investigated in eye imaginal disc of Alzheimer's disease model of *Drosophila* 3rd instar larvae. The in-vivo interaction of **KBH** with  $\text{Cu}^{2+}$  in gut tissues of *Drosophila* larvae establishes its sensing capability in biological system. Interestingly, the in-vivo detection of  $\text{Cu}^{2+}$  has been done using bright field imaging which eliminates the necessity of a fluorescent label, hence making the method highly economical.

## 1. Introduction

Alzheimer's disease (AD), accounting for about 60–80 % of dementia cases, is a neurodegenerative disorder leading to inabilities in thinking, irreversible memory loss, behavioral disorders and severe deterioration of cognitive functions [1]. The disease is characterized by two major neuropathological indications; the deposition of extracellular amyloid  $\beta$  ( $\text{A}\beta$ ) plaques and intracellular neurofibrillary tau tangles (NFT) [2]. Although multiple mechanisms have been reported for AD pathogenesis, the widely acknowledged amyloid cascade hypothesis suggested the accumulation of  $\text{A}\beta$  plaques in the brain as the major incident in AD pathogenesis [3].  $\text{A}\beta$  plaques consist of peptides of 39–43 amino acids. Two polymorphic forms of  $\text{A}\beta$  peptide; fibrillar and oligomeric aggregates have been reported [4]. The longer peptides tend to aggregate easily into insoluble fibrils which are relatively inert. However, the small soluble oligomeric aggregates are believed to be the most neurotoxic and the main agent of the AD pathogenesis. World Health Organization report says that more than 50 million people worldwide suffer from dementia and it is expected to triple during the next 30 years [5]. Despite being a global concern and a century of research, there is still no known cure for the disease. Currently used treatments are limited to slow down the progression of AD and also their efficiency is minimum and short-term [6–8]. However, early diagnosis and

\* Corresponding author.

E-mail address: [singhvp@bhu.ac.in](mailto:singhvp@bhu.ac.in) (V.P. Singh).

monitoring of AD would increase the effectiveness of the treatment methods resulting in reduced mortality and healthcare costs [9]. An early diagnosis of AD is possible as the pathological changes start several years before clinical symptoms appear in patients. The development of AD has been identified in six stages [10]. Stages I and II are considered as preclinical and asymptomatic. Stages III-V are characterized by severe neuronal degeneration and the appearance of first clinical symptoms of AD. Finally, in Stage VI, the disease affects the motor and sensory fields. Unfortunately, mostly the AD is diagnosed when significant damage has occurred in the brain. Therefore there is an urgent need of the early diagnosis of AD in the preclinical stage of its development.

Several studies reported the occurrence of elevated concentrations of biometals in coexistence with A $\beta$  peptide in the senile plaques of an AD brain [11]. Metals like copper, iron and zinc have the tendency to coordinate at metal binding sites of A $\beta$  peptide which accelerates its aggregation and also stabilizes the oligomeric polymorph [12]. In particular, copper imbalance in body has been claimed responsible for the AD pathogenesis, because of its ability to produce reactive oxygen species, which eventually exert oxidative stress and neuronal damage in AD [13,14]. The role of copper in AD is controversial, as in few reports deficiency of copper was observed in AD brain [15–17]. However, a series of scientific evidences have shown the increased level of copper in AD brain [18–20]. Consequently, the detection and monitoring of the increased concentration of copper in the brain could be helpful in the early diagnosis of AD. Hence, we have designed and synthesized a chromogenic probe, **KBH** ((*Z*)-*N*'-(2-amino-5-chlorophenyl)(phenyl)methylene)-2-hydroxybenzohydrazide) to specifically act as copper chelator by extracting copper from Cu-amyloid complex in AD brain.

The first copper chelator ligands used for AD therapy were 8-hydroxyquinoline derivatives, Clioquinol and PBT2 [21]. They were able to bind with copper in A $\beta$  plaques, however, failed due to their lack of efficacy and serious side-effects on long-term use. Further several aminopyrine-based and phenol amino derivatives such as thioflavine-, resveratrol-, coumarin-, and benzothiazole-based compounds have been studied as a promising chelating agent to detect copper in AD patients [22]. Inspired from these chelators, we decided to explore the efficacy of diarylethene moiety as a metal chelator due to its exceptional photophysical properties and chemical stability [23,24]. To the best of our knowledge, no study on the use of diarylethene scaffold as metal chelator in AD brain has been reported. Moreover, several reports have established the Schiff bases as chromophores offering strong bonding with metal ions because of their  $\pi$ -acceptor property [25,26]. Hence, a diarylethene based Schiff base could act as an efficient chromophore for metal ion detection.

Although fluorometric sensing method is widely investigated for the detection of Cu<sup>2+</sup> [27,28], yet they suffer from the limitation of necessity of complex fluorescence active probes and high cost instrumentation. However, colorimetric detection methods offer major advantages including naked-eye recognition, high sensitivity and selectivity, low cost, simple equipment and real-time detection. Label-free colorimetric sensor comprising Au and Ag nanoparticles have been reported for diagnosing AD *via* monitoring A $\beta$  peptides [29]. Hu et al. has reported a nanozyme colorimetric sensor based on (Zn/Fe/Cu)-MnO<sub>2</sub> to observe the development of A $\beta$  aggregates [30]. Inspired from all the development in the field of early diagnosis of AD, we developed **KBH** as a metal chelator to detect the distribution of Cu<sup>2+</sup> *via* bright field imaging in the gut tissues and eye imaginal disc of the AD *Drosophila*. The use of bright field imaging eliminated the limitation to use a fluorescent label, hence made our system an economical and simplified method of detection.

## 2. Experimental

### 2.1. Reagents and instrumentation

All the reagents and solvents were obtained from Sigma-Aldrich Chemicals, USA. Milli-Q water used in the experiments was freshly prepared. <sup>1</sup>H and <sup>13</sup>C NMR spectra were recorded in DMSO-*d*<sub>6</sub> on Bruker India Scientific (Model-Avance Neo 600 MHz) multinuclear spectrometer. FT-IR and HRMS spectra were recorded on FT/IR-4700 JASCO spectrophotometer and HRMS SCIEX X-500R QTOF, respectively. The single crystal X-ray diffraction data was recorded on XtaLAB Synergy-I diffractometer and the structure refinement and solution was carried out using Olex2 and SHELXTL program. A fluorescent microscope with NIS-Element BR4.30064 bit software was used to capture the images of *Drosophila*.

### 2.2. Synthesis of **KBH**

In a round bottomed flask, a solution of 2-hydroxybenzohydrazide (0.152 g, 1 mmol) in methanol was mixed with the methanolic solution of 2-amino-5-chlorobenzophenone (0.231 g, 1 mmol) slowly with stirring and refluxed for 5 h. The reaction mixture was evaporated to obtain a yellow solid. Recrystallization was done in DMSO and the obtained yellow crystals (Yield 90 %) were filtered and dried. m.p. 245 °C. <sup>1</sup>H NMR (DMSO-*d*<sub>6</sub>,  $\delta$  in ppm): 11.08 (s, 1H, NH), 10.90 (s, 1H, OH), 7.96–6.49 (12H, Ar-H), 7.67 (br, 2H, NH<sub>2</sub>); <sup>13</sup>C NMR (DMSO-*d*<sub>6</sub>): 161.40 (C=O), 156.19 (C=N), 155.71–117.04 (Ar-C). IR ( $\nu$  cm<sup>-1</sup>): (OH) 3486, (NH) 3285, (C=O) 1621, (C=N) 1614, (N-N) 975; *Anal. Calc.* for C<sub>20</sub>H<sub>16</sub>N<sub>3</sub>O<sub>2</sub>Cl (365.0931): HRMS *m/z*: 366.0983 [M + H]<sup>+</sup>.

### 2.3. Spectroscopic experiments

The stock solutions (10<sup>-2</sup> M) of **KBH** and metal salts in DMSO and Milli-Q water, respectively, were used for all the experiments. HEPES buffer (pH 7.4) was used as the sensing medium. UV-Vis titration data was used to calculate the binding constant (K<sub>b</sub>) of **KBH**-Cu<sup>2+</sup> by Benesi-Hildebrand plot equation (1).

$$1 / (A - A_0) = 1 / (K_a (A_{max} - A_0) [Metal]) + 1 / (A_{max} - A_0). \quad (1)$$

where,  $A$  and  $A_0$  are the **KBH** absorbance values, with and without  $\text{Cu}^{2+}$ , respectively;  $A_{\text{max}}$  is the **KBH** maximum absorbance value with excess of  $\text{Cu}^{2+}$ .  $[\text{Metal}]$  is the concentration of  $\text{Cu}^{2+}$ . The limit of detection (LOD) was calculated by using equation (2), where  $\sigma$  is the standard deviation.

$$\text{LOD} = 3\sigma / \text{slope} \quad (2)$$

## 2.4. Biological experiments

### 2.4.1. *Drosophila* stocks and culture details

*Drosophila* stocks were obtained from Bloomington *Drosophila* Stock Center, Indiana, USA. The fly stocks used were OregonR<sup>+</sup> as wild type, ey-GAL4/CyO as driver line and UAS-Abeta-ey-Gal4/CyO as responder line. The AD model was generated using ey-GAL4/CyO and UAS-Abeta-ey-Gal4/CyO flies. The culture of fly stocks was done in corn agar media at  $28 \pm 1$  °C in a BOD incubator.

### 2.4.2. Toxicity assay

The control flies were fed with normal food, whereas the test flies were exposed to various concentrations (50, 100 and 200  $\mu\text{M}$ ) of **KBH**,  $\text{Cu}^{2+}$  and **KBH** +  $\text{Cu}^{2+}$  in each group for the median lethal dose ( $\text{LD}_{50}$ ) determination. The growth of OregonR<sup>+</sup> f1 progeny was monitored after 20 days of treatment.

### 2.4.3. Cell viability assay

Cell viability of 3rd instar larval gut tissues was observed using MTT assay. Larval gut was dissected ( $n = 10$  in each group) and treated with 50, 100 and 200  $\mu\text{M}$  of **KBH**,  $\text{Cu}^{2+}$  and **KBH** +  $\text{Cu}^{2+}$  in the cavity slides in 1xPBS under stereo binocular microscope. The gut tissues were washed thrice with 1xPBS and incubated in 0.6 mg/ml MTT in 100  $\mu\text{l}$  at 37 °C for 2 h. The MTT was removed and the tissues were washed with 1xPBS twice. Then added 100  $\mu\text{l}$  DMSO and dissolved in the formazan crystal. The absorbance was recorded at 575 nm by a multi-mode plate reader.

### 2.4.4. In-vivo interaction of **KBH** with $\text{Cu}^{2+}$ in gut tissues and eye disc of AD *Drosophila*

The larvae ( $n = 10$  of each group) were dissected in 1xPBS and the tissues were fixed in 4 % paraformaldehyde for 20 min. After washing thrice with 1xPBS, the tissues were incubated in **KBH**,  $\text{Cu}^{2+}$  and **KBH** +  $\text{Cu}^{2+}$  for 10 min. Again the tissues were washed with 1xPBS thrice and then mounted on slides in DABCO. Finally, the images were captured on a Nikon-NiU fluorescence microscope.

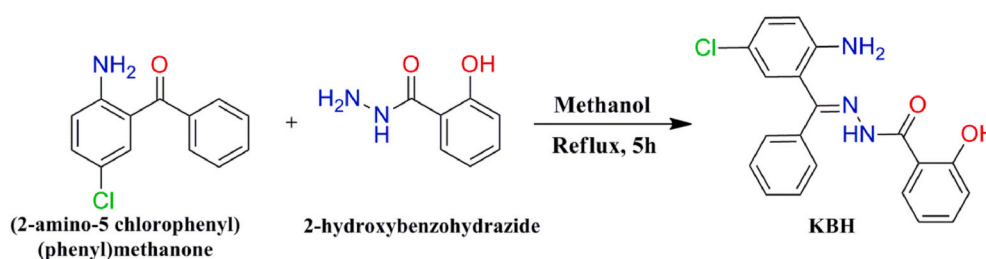
## 3. Results and discussion

### 3.1. Synthesis and spectral characterization of **KBH**

The **KBH** was synthesized efficiently using a facile procedure [31] as shown in Scheme 1. The final product was characterized by  $^1\text{H}$  and  $^{13}\text{C}$  NMR, FT-IR and HRMS. The molecular structure of the probe was established using single crystal X-ray diffraction technique for the first time.

$^1\text{H}$  NMR spectrum of **KBH** presented the N–H and O–H protons peaks at 11.08 and 10.90 ppm, respectively. The multiplets in the range of 7.96–6.49 ppm showed the existence of aromatic protons (Fig. S1).  $^{13}\text{C}$  NMR spectrum of **KBH** displayed the distinguishing peaks of C=O and C=N carbons at 161.40 and 156.19 ppm, respectively (Fig. S2). The IR bands appeared at 3486, 3285 and 1621  $\text{cm}^{-1}$  ascribed to O–H, N–H and C=O bonds, respectively. The band at 1614  $\text{cm}^{-1}$  confirmed the imine (>C=N-) group (Fig. S3). HRMS spectrum (Fig. S4) showed a molecular ion peak at  $m/z$  366.0983  $[\text{M}+\text{H}]^+$ .

The single crystal structural refinement data of the probe, **KBH** has been shown in Table 1. It existed as a monoclinic crystal system ( $a = 12.5067(4)$  Å,  $b = 8.1302(2)$  Å and  $c = 19.0534(5)$  Å) with  $P2_1/c$  space group. Fig. 1 represented the ORTEP structure of **KBH** and the related bond lengths and bond angles has been presented in Tables S1 and S2. Structure of **KBH** is stabilized due to intramolecular (N2–H2–O1, 1.98 Å) and intermolecular (O1–H1...O3', 1.87 Å) hydrogen bonding. The double bond character of O2–C14 and N1–C7 bonds were confirmed by their bond lengths of 1.225 and 1.281 Å, respectively.



Scheme 1. Synthesis route for **KBH**.

**Table 1**  
Crystallographic data and structure refinement for **KBH**.

Empirical formula	C <sub>21</sub> H <sub>19</sub> ClN <sub>3</sub> O <sub>3</sub>
Formula weight	396.84
Temperature/K	293(2)
Crystal system	monoclinic
Space group	P2 <sub>1</sub> /c
a/Å	12.5067(4)
b/Å	8.1302(2)
c/Å	19.0534(5)
α/°	90
β/°	94.993(3)
γ/°	90
Volume/Å <sup>3</sup>	1930.04(9)
Z	4
ρ <sub>calc</sub> /cm <sup>3</sup>	1.369
μ/mm <sup>-1</sup>	0.225
F(000)	828.0
Crystal size/mm <sup>3</sup>	0.30 × 0.25 × 0.05
Radiation	Mo Kα (λ = 0.71073)
2θ range for data collection/°	5.164 to 54.272
Index ranges	−15 ≤ h ≤ 16, −10 ≤ k ≤ 10, −24 ≤ l ≤ 23
Reflections collected	42121
Independent reflections	4123 [R <sub>int</sub> = 0.0483, R <sub>sigma</sub> = 0.0303]
Data/restraints/parameters	4123/0/268
Goodness-of-fit on F <sup>2</sup>	1.075
Final R indexes [I ≥ 2σ (I)]	R <sub>1</sub> = 0.0425, wR <sub>2</sub> = 0.1141
Final R indexes [all data]	R <sub>1</sub> = 0.0585, wR <sub>2</sub> = 0.1233
Largest diff. peak/hole/e Å <sup>-3</sup>	0.55/−0.27

$${}^a R_1 = \frac{\sum ||F_o| - |F_c||}{\sum |F_o|}$$

$${}^b R_2 = \left[ \frac{\sum w(|F_o|^2 - |F_c|^2)^2}{\sum w|F_o|^2} \right]^{1/2}$$

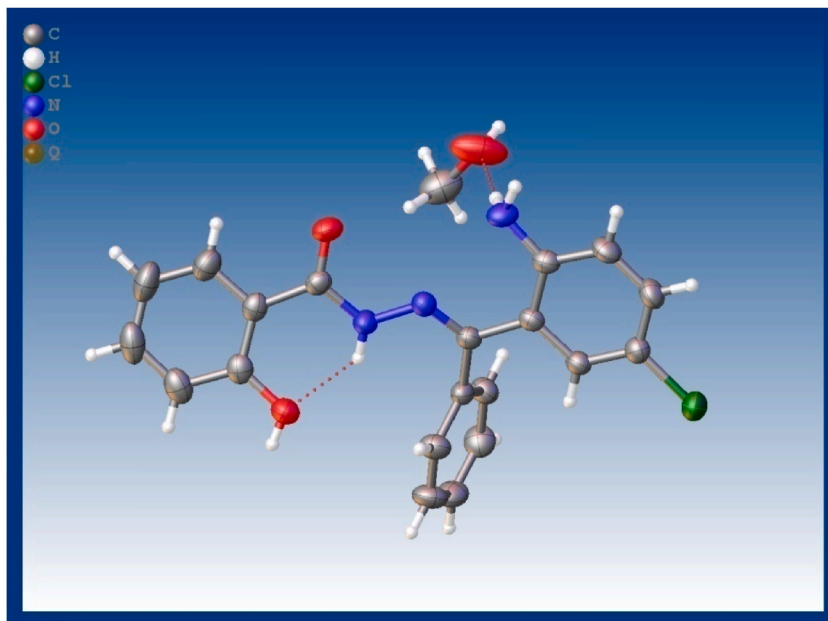


**Fig. 1.** ORTEP image of **KBH**.

### 3.2. UV–Vis absorption studies of **KBH** with Cu<sup>2+</sup>

Prior to performing the in vivo experiments, we optimized all the sensing parameters. Preliminary colorimetric investigations were conducted with **KBH** and a series of metal ions to examine the metal ion recognition ability of **KBH**. The solutions of **KBH** (30 μM) and metal ions (30 μM) were added in 1:1 ratio in HEPES buffer and an immediate colour change from colourless to yellow occurred with Cu<sup>2+</sup> only (Fig. 2a). Other cations were ineffective to produce any colour change in **KBH** solution. From this naked eye experiment, the

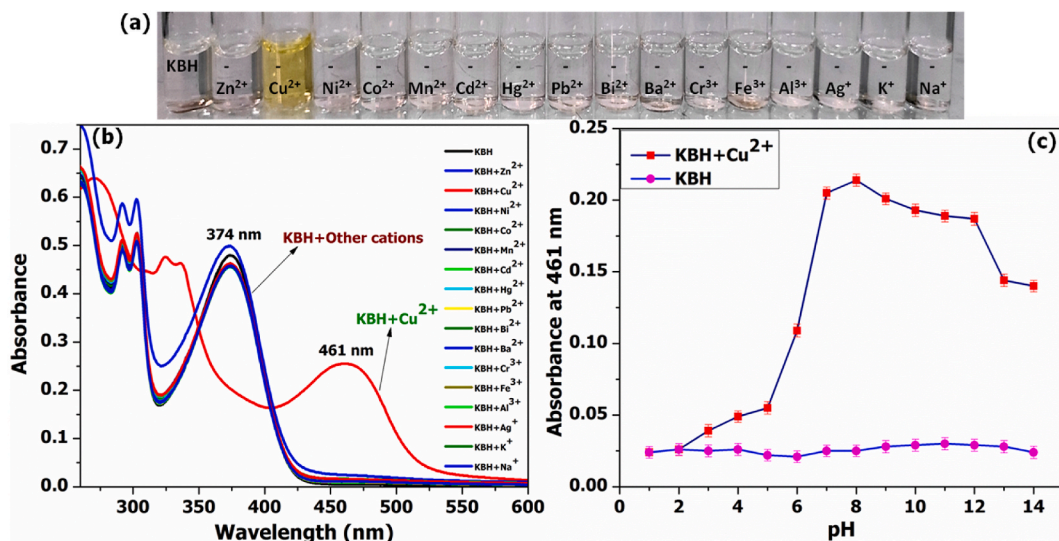


Fig. 2(a). Visible colour change and (b) UV-Vis absorption spectra of KBH (30 μM) after the addition of other metal ions (30 μM) in HEPES buffer (c) effect of pH variation (error bars for  $n = 3$ ). (For interpretation of the references to colour in this figure legend, the reader is referred to the Web version of this article.)

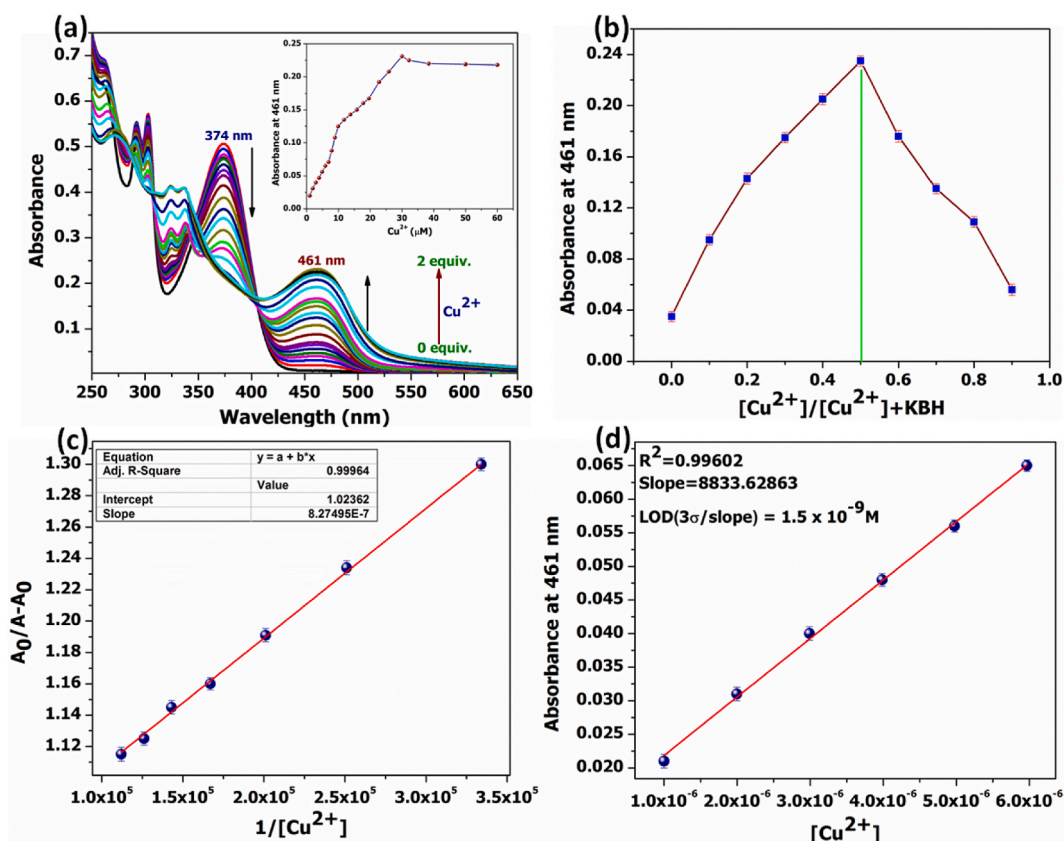


Fig. 3. (a) UV-Vis titration spectra of KBH (30 μM) on increasing addition of Cu<sup>2+</sup> (0-2 equiv.) in HEPES buffer (pH 7.4). (b) Job's plot for KBH-Cu<sup>2+</sup> complex. (c) Binding constant of KBH with Cu<sup>2+</sup> was 0.12 × 10<sup>7</sup> M<sup>-1</sup> (R<sup>2</sup> = 0.99964). (d) LOD was calculated as 1.5 × 10<sup>-9</sup> M (R<sup>2</sup> = 0.99602). Error bars for  $n = 3$ .

sensing ability of **KBH** for  $\text{Cu}^{2+}$  ions was established. The UV–Vis absorption spectrum of **KBH** (30  $\mu\text{M}$ ) in HEPES buffer displayed an absorption peak at 374 nm due to  $n\text{-}\pi^*$  transition [32]. After the addition of  $\text{Cu}^{2+}$ , the intensity of the absorption peak at 374 nm disappeared and a new peak originated at 461 nm. The appearance of new band could be due to intramolecular charge transfer (ICT) between **KBH** and  $\text{Cu}^{2+}$  [33]. The sensing efficiency of **KBH** (30  $\mu\text{M}$ ) towards  $\text{Cu}^{2+}$  was established by recording UV–Vis absorption spectrum in the presence of various metal ions (30  $\mu\text{M}$ ) including  $\text{Zn}^{2+}$ ,  $\text{Cu}^{2+}$ ,  $\text{Ni}^{2+}$ ,  $\text{Co}^{2+}$ ,  $\text{Mn}^{2+}$ ,  $\text{Cd}^{2+}$ ,  $\text{Hg}^{2+}$ ,  $\text{Pb}^{2+}$ ,  $\text{Bi}^{2+}$ ,  $\text{Ba}^{2+}$ ,  $\text{Cr}^{3+}$ ,  $\text{Fe}^{3+}$ ,  $\text{Al}^{3+}$ ,  $\text{Ag}^+$ ,  $\text{K}^+$  and  $\text{Na}^+$  in HEPES buffer (Fig. 2b). No observable change was observed in the spectrum of **KBH** with other metal ions.

Further, the stability of **KBH** and its sensing ability towards  $\text{Cu}^{2+}$  in various pH environments was examined. The absorption spectra of **KBH** (30  $\mu\text{M}$ ) and  $\text{Cu}^{2+}$  (30  $\mu\text{M}$ ) in different pH solutions (pH 1–14, HEPES buffer) were recorded (Fig. 2c). **KBH** alone showed great inertness in various pH environments and no observable change was seen in its absorption maxima. This also indicated that its sensing ability was because of the  $\text{Cu}^{2+}$  interaction only. However, the absorbance of **KBH**– $\text{Cu}^{2+}$  was greatly reduced at acidic and highly basic pH. The maximum sensing efficiency of **KBH** was seen in the pH range from 7 to 12. Hence, **KBH** was proved to be highly compatible to effectively work in the biological environment. As our motive was to use **KBH** in biological systems, we performed all the experiments at pH 7.4.

### 3.3. UV–Vis titration, Job's plot, binding constant and LOD

Further the UV–Vis titration experiment was performed to determine the binding constant and LOD of **KBH** towards  $\text{Cu}^{2+}$ . To conduct the experiment, absorption spectra of **KBH** (30  $\mu\text{M}$ ) were recorded with increasing concentration of  $\text{Cu}^{2+}$  solution. As shown in Fig. 3a, with increasing concentration of  $\text{Cu}^{2+}$  (0–2.0 equiv.), the intensity of absorption peak at 374 nm was seen decreasing, whereas, a linear increase in the intensity of the newly originated band at 461 nm was observed. No further increase in absorption intensity was found with excess amount of  $\text{Cu}^{2+}$  ions. Job's plot determined the 1:1 stoichiometry of **KBH**– $\text{Cu}^{2+}$  with intensity maximum at 0.5 mol fraction of  $\text{Cu}^{2+}$  (Fig. 3b). From the UV–Vis titration data, binding constant ( $K_a$ ) and LOD for the **KBH**– $\text{Cu}^{2+}$  were calculated by using Benesi-Hildebrand equation [34] and found to be  $0.12 \times 10^7 \text{ M}^{-1}$  (Figs. 3c) and  $1.5 \times 10^{-9} \text{ M}$  (Fig. 3d), respectively. The observed low detection limit indicated that **KBH** is best suited for biological analysis, and hence, can meet the practical demands.

### 3.4. Competitive experiment

To establish **KBH** as a highly selective practical tool for colorimetric sensing of  $\text{Cu}^{2+}$  in biological systems, competitive experiments were conducted (Fig. 4). Absorption spectra of **KBH** (30  $\mu\text{M}$ ) were recorded in the presence of  $\text{Cu}^{2+}$  ions (1 equiv.) in addition to other metal ions (5 equiv.) in HEPES buffer (pH 7.4). No significant interference of other metal ions was observed for the detection of  $\text{Cu}^{2+}$ . The selectivity of **KBH** for  $\text{Cu}^{2+}$  indicated that it will not disturb the metal balance of the biological system by binding with other coexisting metal ions.

### 3.5. Reversibility study

The reversibility of a chemosensor is an essential requirement to examine the variation in the analyte concentration. Therefore, reversibility studies were performed by adding EDTA (30  $\mu\text{M}$ ) to in-situ generated **KBH**– $\text{Cu}^{2+}$  in HEPES buffer (pH 7.4).

With the addition of EDTA, a colour change from yellow to colourless was observed. This reversibility of the **KBH**– $\text{Cu}^{2+}$  was due to

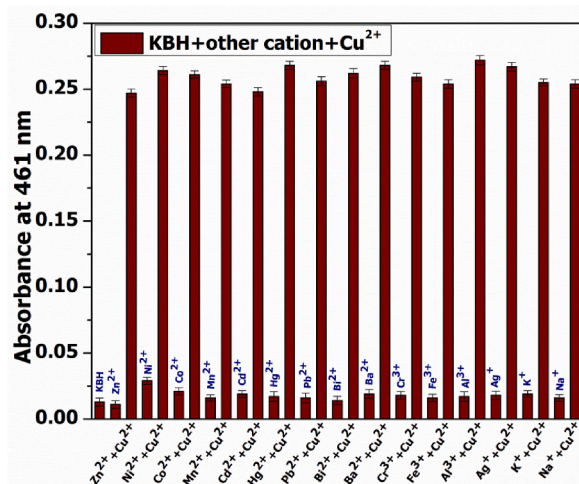


Fig. 4. Competitive experiment of **KBH** (30  $\mu\text{M}$ ) and  $\text{Cu}^{2+}$  (1 equiv.) with various metal ions (5 equiv.) in HEPES buffer (pH 7.4, error bars for  $n = 3$ ).

the stronger binding affinity of  $\text{Cu}^{2+}$  towards EDTA. No significant change in absorption spectrum of **KBH** was observed with EDTA, whereas, the sensing property was completely reversed by adding EDTA to **KBH**- $\text{Cu}^{2+}$ . After adding EDTA, the **KBH**- $\text{Cu}^{2+}$  spectrum reversed back to the **KBH** spectrum (Fig. 5a). Further, the reversibility of **KBH** was investigated by alternate additions of  $\text{Cu}^{2+}$  and EDTA to the **KBH**. This resulted in corresponding appearance and disappearance of the yellow colour. This cycle was repeated 4 times to validate the reversibility (Fig. 5b).

The reversible response of **KBH**- $\text{Cu}^{2+}$  with EDTA encouraged to examine its selectivity towards other anions (30  $\mu\text{M}$ ) such as  $\text{CN}^-$ ,  $\text{HCO}_3^-$ ,  $\text{Cl}^-$ ,  $\text{SO}_3^{2-}$ ,  $\text{ClO}_4^-$ ,  $\text{CO}_3^{2-}$ ,  $\text{NO}_2^-$ ,  $\text{SCN}^-$ ,  $\text{SO}_4^{2-}$ ,  $\text{OH}^-$ ,  $\text{CH}_3\text{COO}^-$  in HEPES buffer (pH 7.4). Fig. 6 showed no significant interference of other anions indicating the selectivity of **KBH**- $\text{Cu}^{2+}$  for EDTA among several anions.

### 3.6. Proposed binding mechanism by FT-IR, $^1\text{H}$ NMR titration and HRMS

#### 3.6.1. Synthesis of **KBH**- $\text{Cu}^{2+}$ complex

The **KBH**- $\text{Cu}^{2+}$  complex was synthesized in a round bottom flask by adding 30 ml methanolic solution of copper(II) nitrate (1 mmol) to 30 ml methanolic solution of **KBH** (1 mmol) slowly with stirring. The reaction mixture was then stirred for 2 h at room temperature. The obtained light green solid was centrifuged, washed with methanol several times and dried (Scheme 2).

To determine the binding sites of **KBH**, FT-IR spectra of **KBH** and the synthesized **KBH**- $\text{Cu}^{2+}$  were compared (Fig. S3). In **KBH** spectrum, the peaks at 3486, 3285 and 3231  $\text{cm}^{-1}$  corresponded to the O-H, N-H and  $\text{NH}_2$  groups, respectively. The distinguishing peaks of C=O and C=N groups in **KBH** appeared at 1621 and 1614  $\text{cm}^{-1}$ , respectively. After complexation with  $\text{Cu}^{2+}$ , the disappearance of N-H and C=O peaks in the spectrum of **KBH**- $\text{Cu}^{2+}$  indicated the involvement of N-H proton in enolization of C=O (amide) and subsequent deprotonation for binding with  $\text{Cu}^{2+}$ . This was supported by the generation of a new peak at 1377  $\text{cm}^{-1}$  corresponding to C-O group. However, O-H and  $\text{NH}_2$  groups were not found to participate in bonding. A shift at lower wave number (1594  $\text{cm}^{-1}$ ) in the  $\nu(\text{C}=\text{N})$  of complex suggested the coordination of C=N group with  $\text{Cu}^{2+}$ .

For more detailed investigation of the binding interaction of **KBH** with  $\text{Cu}^{2+}$ ,  $^1\text{H}$  NMR titration was performed. The spectra of **KBH** were recorded in  $\text{DMSO}-d_6$  by adding 0–1.0 equiv. of  $\text{Cu}(\text{NO}_3)_2 \cdot 3\text{H}_2\text{O}$ . Although all the proton peaks were broadened due to the paramagnetic behaviour of  $\text{Cu}^{2+}$ , but still their positions could be compared with free **KBH**. With the increasing concentration of  $\text{Cu}^{2+}$ , the NH proton peak at 11.08 ppm decreased gradually and disappeared at 1 equiv.  $\text{Cu}^{2+}$ . The chemical shift values of O-H and  $\text{NH}_2$  protons at 10.90 and 7.67 ppm respectively, were unaffected upon complexation. No change in the position of aromatic protons was observed (Fig. S5). These observations also suggested the involvement of N-H proton in enolization of amide C=O group. Hence, it is evident that imine-N and amide-O are the binding sites of **KBH**. Based on FT-IR,  $^1\text{H}$  NMR titration and Job's plot, a four coordinated structure of **KBH**- $\text{Cu}^{2+}$  was proposed as shown in (Scheme 2). The chelation of  $\text{Cu}^{2+}$  with the enol form of **KBH** increased the charge transfer, hence resulting in the red shift (87 nm) of the absorbance band. In HRMS spectrum of **KBH**- $\text{Cu}^{2+}$ , the peak at 511.0655  $[\text{M}+\text{Na}]^+$  (Fig. S6) validated its structure.

### 3.7. Theoretical investigation

Computational calculations were performed to investigate the binding mode and the relative energies of HOMO-LUMO of **KBH** and **KBH**- $\text{Cu}^{2+}$  by density functional theory (DFT) method. The ground state geometries of **KBH** (Fig. S7a) and **KBH**- $\text{Cu}^{2+}$  (Fig. S7b) were theoretically optimized using Gaussian 09 computational program with B3LYP function using the 6-311G(d, p) basis set [35].

A comparison of the energy of HOMO and LUMO of **KBH** and **KBH**- $\text{Cu}^{2+}$  indicated that the complexation of **KBH** with  $\text{Cu}^{2+}$  lead to the more stabilized orbitals. After complexation, a decrease in the energy gap between the HOMO and LUMO was observed from 4.12 to 3.22 eV, inferring the increased stabilization of the complex. This stabilization was also reflected by the bathochromic shift in

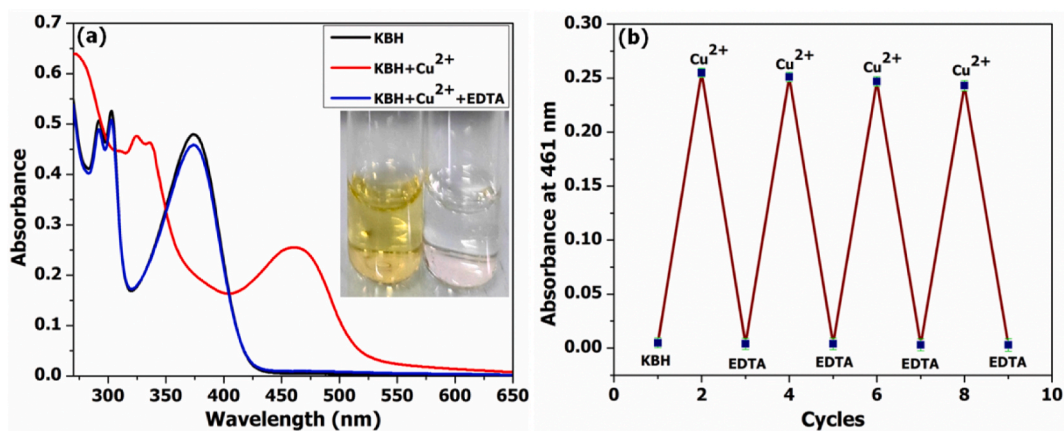
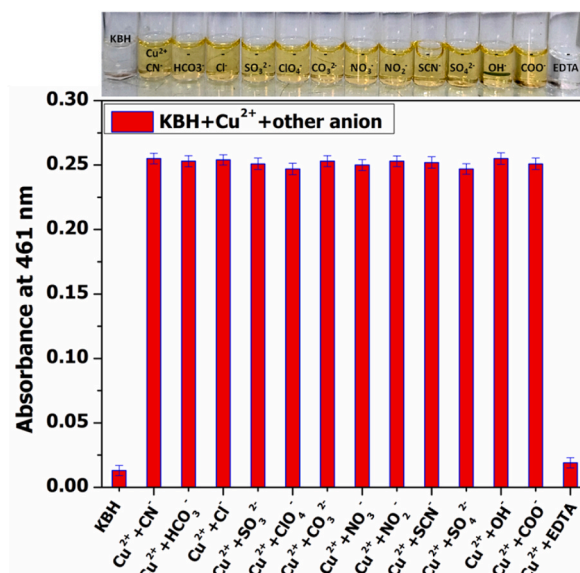
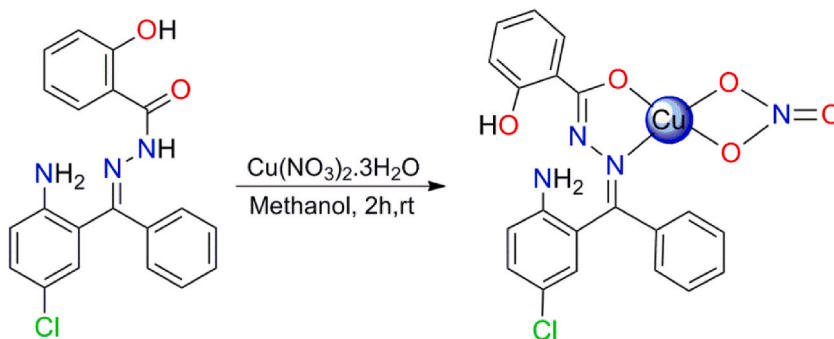


Fig. 5(a). Reversibility spectra of **KBH**- $\text{Cu}^{2+}$  (30  $\mu\text{M}$ ) with EDTA (30  $\mu\text{M}$ ) in HEPES buffer (pH 7.4). (b) Reversibility cycle of **KBH** with  $\text{Cu}^{2+}$  and EDTA, alternatively (error bars for  $n = 3$ ).



**Fig. 6.** Top Visible colour change and **Bottom:** UV-Vis spectra of  $\text{KBH-Cu}^{2+}$  (30  $\mu\text{M}$ ) with other anions (30  $\mu\text{M}$ ) in HEPES buffer (pH 7.4, error bars for  $n = 3$ ). (For interpretation of the references to colour in this figure legend, the reader is referred to the Web version of this article.)



**Scheme 2.** Synthesis route for  $\text{KBH-Cu}^{2+}$ .

absorption wavelength of  $\text{KBH}$ . As shown in Fig. 7, before complexation the HOMO electron density was oriented over the diarylethene moiety of  $\text{KBH}$  which was transferred to hydroxy-phenyl ring after binding with  $\text{Cu}^{2+}$ , indicating the intramolecular charge transfer (ICT). The bond length and bond angles of  $\text{KBH}$  and  $\text{KBH-Cu}^{2+}$  were obtained from geometry optimized structures. Upon coordination with  $\text{Cu}^{2+}$ , the bond length of  $\text{C=O}$  increased from 1.214 to 1.283 Å, whereas, a decrease in the bond length of amide  $\text{C-N}$  from 1.411 to 1.342 Å was observed. These observations also supported the enolization of  $\text{KBH}$  during complexation. The bond angles of  $\text{O=C-N}$  and  $\text{C=N-N}$  in  $\text{KBH}$  were found to be 123.26° and 120.11° which after complexation changed to 123.13° and 117.20°, respectively. The observed changes in bond angles of  $\text{KBH}$  upon coordination with  $\text{Cu}^{2+}$  further validated the binding of  $\text{KBH}$  via amide-O and imine-N.

### 3.8. Test kit and real water sample analysis

To establish  $\text{KBH}$  as a practical tool for detection of  $\text{Cu}^{2+}$ , we developed an economical and easy to use paper strip kit. The test strips were prepared by coating filter paper with  $\text{KBH}$  (30  $\mu\text{M}$ ) solution. These test strips were then dipped into  $\text{Cu}^{2+}$  solution (30  $\mu\text{M}$ ) exhibiting the colour change from colourless to yellow (Fig. 8a).

Encouraged by the colorimetric response of  $\text{KBH}$ , we tested its efficiency for the detection of  $\text{Cu}^{2+}$  in real water samples. Tap water and Ganga river water were spiked with various concentrations of  $\text{Cu}^{2+}$  (4.9, 9.9, 15.7, 19.6, 25.9  $\mu\text{M}$ ) and a blank solution of  $\text{KBH}$  in HEPES buffer (pH 7.4) was used as control [36]. With the standard titration plot in Fig. 3a, the recovery percentage was calculated by equation (3) as:

$$\text{Percentage recovery} = \frac{[S] - [B]}{[SS]} \times 100 \quad (3)$$

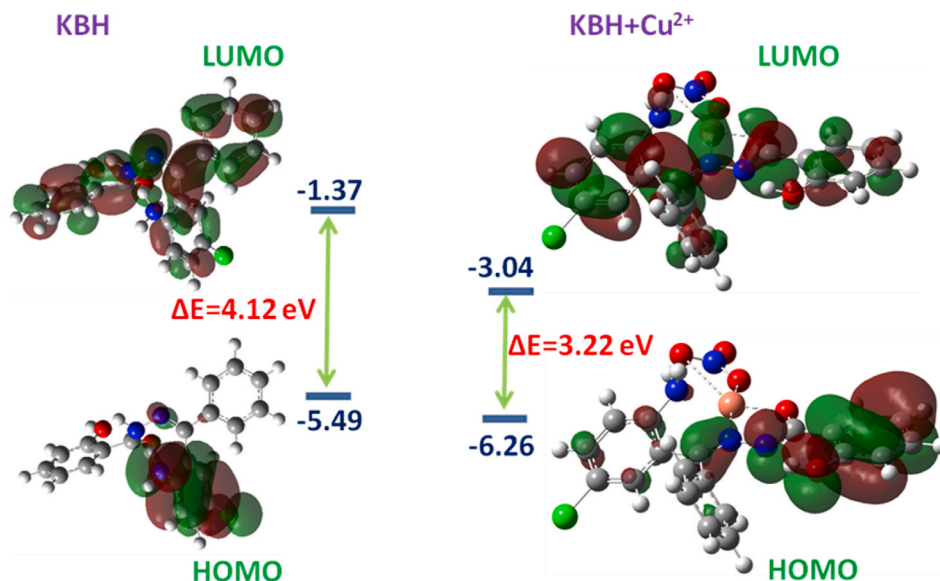


Fig. 7. Optimized energy gap in HOMO and LUMO of KBH and KBH–Cu<sup>2+</sup>.

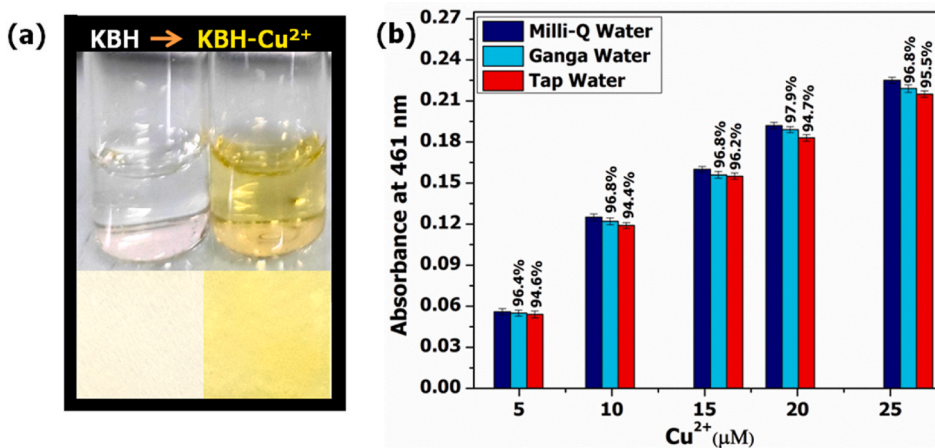


Fig. 8(a). Paper strip kit. (b) Real sample analysis of Cu<sup>2+</sup> in tap and Ganga river water (error bars for n = 3).

where [S] and [B] are the KBH absorbance values, with or without Cu<sup>2+</sup>, respectively and [SS] is KBH–Cu<sup>2+</sup> absorbance in standard solution (HEPES buffer, pH 7.4). The calculated recovery percentages (Fig. 8b) indicated that sensing property of KBH was unaffected by the coexisting molecules.

### 3.9. In-vivo study of KBH interaction with Cu<sup>2+</sup> in gut tissues of AD Drosophila

Prior to explore the Cu<sup>2+</sup> detection efficiency of KBH in the biological system, the measurement of its toxicity to the tissues was required. Hence, the toxic behaviour of KBH, Cu<sup>2+</sup> and KBH–Cu<sup>2+</sup> was checked in OregonR + F1 progeny. The F1 progeny of control showed 100 % eclosion of flies. The F1 progeny treated with 50 μM of KBH showed no larval and pupal deaths with 78 % of eclosed flies (Fig. 9a). However, with increasing concentration of KBH, a reduction in the eclosion of flies was observed. Similarly, 50 μM concentration of Cu<sup>2+</sup> and KBH–Cu<sup>2+</sup> also didn't show any toxicity for fly development with 91 and 92 % of eclosed flies, respectively (Fig. 9b and c).

Further, the MTT assay was carried out to examine the cell viability of larval gut tissues treated with various concentrations of KBH, Cu<sup>2+</sup> and KBH + Cu<sup>2+</sup>. The control flies showed 100 % cell viability. The gut tissues treated with KBH showed good cell viability at all the tested concentrations (Fig. 9d). However, the Cu<sup>2+</sup> and KBH + Cu<sup>2+</sup> treated larval gut tissues exhibited a reduced percentage of cell viability as compared to control (Fig. 9e and f). These results showed that concentration of 50 μM can be used for further experiments due to its non-toxicity for flies.

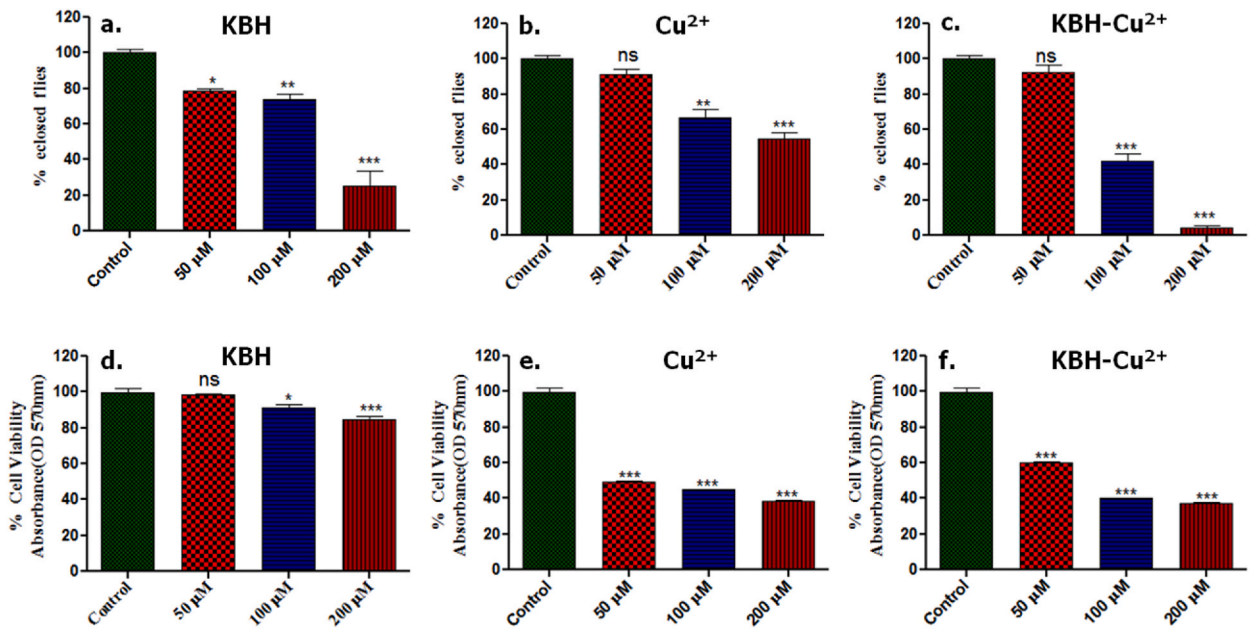


Fig. 9(a, b and c). The development of OregonR<sup>+</sup> flies and (d, e and f) % of cell viability in gut tissues of AD *Drosophila* 3rd instar larvae on various concentrations of KBH, Cu<sup>2+</sup> and KBH-Cu<sup>2+</sup>. The data were analyzed by one-way ANOVA and error bars for n = 3.

To explore the in vivo interaction of KBH with Cu<sup>2+</sup>, the bio-imaging experiment under bright field in gut tissues of AD *Drosophila* 3rd instar larvae was performed. The larvae fed with normal food, Cu<sup>2+</sup> and KBH alone showed no colour in gut tissues (Fig. 10a, b, c). Most importantly, the KBH treated tissues when administered with Cu<sup>2+</sup>, displayed a yellow colour (Fig. 10d). This indicated that KBH could detect Cu<sup>2+</sup> in gut tissues, hence confirmed its in-vivo sensitivity and selectivity towards Cu<sup>2+</sup> ions in the biological environment.

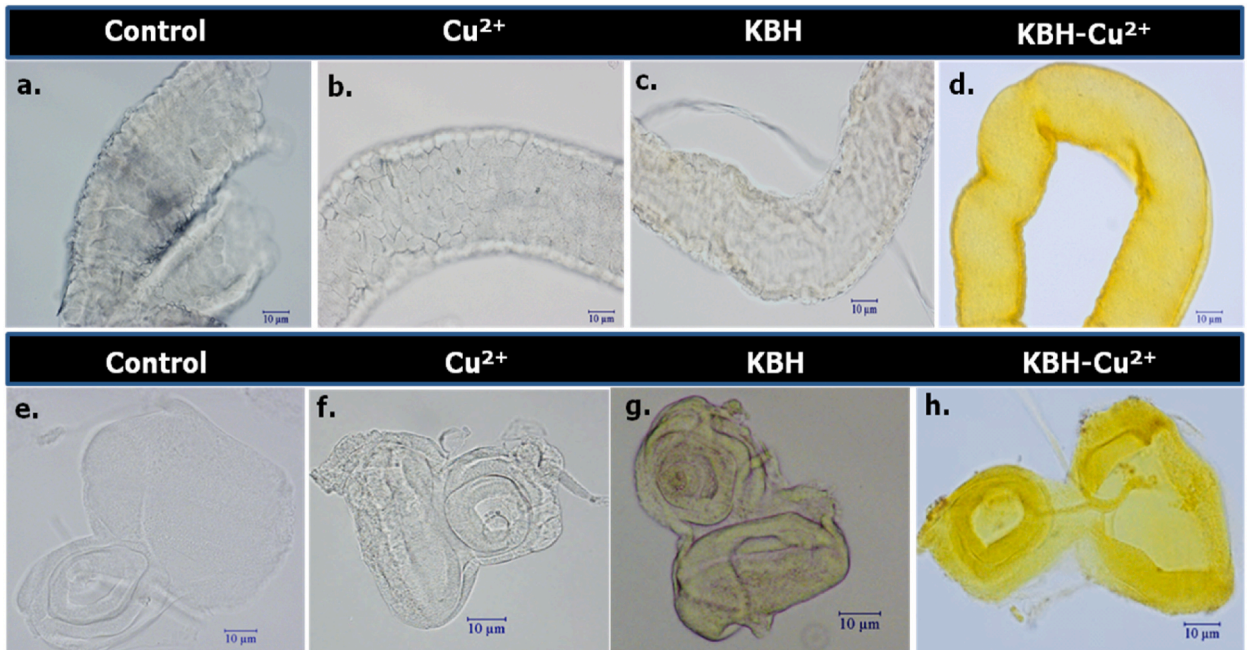


Fig. 10. The 3rd instar larval gut tissues shows no colour in (a) untreated, (b) Cu<sup>2+</sup>-treated, (c) KBH- treated flies and yellow colour in (d) KBH-Cu<sup>2+</sup>-treated flies. The 3rd instar larval eye imaginal disc shows no colour in (e) untreated, (f) Cu<sup>2+</sup>-treated flies and light yellow colour in (g) KBH- treated and intense yellow colour in (h) KBH-Cu<sup>2+</sup>-treated flies. Scale bars are 10 μm. (For interpretation of the references to colour in this figure legend, the reader is referred to the Web version of this article.)

### 3.10. In-vivo study of **KBH** interaction with $\text{Cu}^{2+}$ in eye disc of *AD Drosophila*

*Drosophila*'s 50 % gene homology with humans and short life cycle offers an attractive model for the accelerated therapeutic and diagnostic study of Alzheimer's like neurodegenerative diseases [37]. The highly organized compound eye of *Drosophila* containing more than 60 % of brain nerve cells develops from an eye-antennal imaginal disc inside the larvae. The eye-antennal imaginal disc grows and differentiates into the pupal retina and later into the adult eye comprising of many unit eyes known as ommatidia. Hence it could be used as an excellent model to study the cause, progression and cure of neurodegeneration [38].

Subsequently, we have established a model system of transgenic *AD Drosophila* using ey-GAL4/CyO driver strains for misexpressing  $\text{A}\beta_{42}$  protein in the eye imaginal disc of the 3rd instar larvae [39]. The transgenic flies exhibited neurodegenerated phenotype in their eye imaginal disc. As discussed earlier, the accumulation of  $\text{A}\beta_{42}$  aggregates in AD patients is characterized by high concentration of metals such as copper [40]. Hence, to examine the presence of  $\text{Cu}^{2+}$  in  $\text{A}\beta_{42}$  aggregates accumulated in the eye imaginal disc of the *AD Drosophila*, bio-imaging experiments were performed. The eye imaginal discs incubated in normal (Fig. 10e) and  $\text{Cu}^{2+}$  treated food (Fig. 10f) showed no colouration. However, the discs treated with **KBH** showed light yellow colour representing the formation of the **KBH**- $\text{Cu}^{2+}$  complex (Fig. 10g), hence indicating the presence of  $\text{Cu}^{2+}$  in  $\text{A}\beta_{42}$  aggregates. Further the **KBH** incubated discs were administered with  $\text{Cu}^{2+}$  solution, resulting in the more intense yellow colour (Fig. 10h). Previously, **KBH** incubated gut tissues of the 3rd instar larvae showed no colouration indicating the absence of  $\text{Cu}^{2+}$  in gut tissues of AD flies (Fig. 10c). The above bio-imaging experiments established **KBH** as a promising chromophore to be used in the early diagnosis of AD.

### 3.11. Comparison with the reported sensors

A comparison table has been incorporated to determine the efficiency of **KBH** as a  $\text{Cu}^{2+}$  sensor with respect to other reported colorimetric probes (Table 2). The results clearly indicated that other reported methods used toxic solvents as sensing medium, whereas **KBH** worked in aqueous medium. **KBH** showed a very attractive LOD value, hence proved to be highly sensitive for  $\text{Cu}^{2+}$ . Additionally, none of the compared methods showed the MTT assay of the probe, however **KBH** was established as a non toxic probe for biological system by performing toxicity and cell viability assays. Most importantly, the majority of past sensors showed the purpose for real water sample analysis, whereas **KBH** in addition to real water sample analysis was also used for the AD diagnostic study and bio-imaging in *Drosophila* model. Hence, it showed great potential to be a capable probe for colorimetric detection of  $\text{Cu}^{2+}$  in various ecological and biological environments.

## 4. Conclusions

In summary, a diarylethene based chemosensor **KBH** was synthesized and characterized by various spectroscopic techniques. It exhibited a great selectivity towards  $\text{Cu}^{2+}$  in aqueous medium with an extremely low limit of detection value. Furthermore, **KBH** was found highly reversible with EDTA. Binding mechanism was proposed by Job's plot, FT-IR,  $^1\text{H}$  NMR titration, HRMS and DFT studies. The practical applicability of **KBH** was shown by real water sample analysis and test strip kit. Bio-imaging in *Drosophila* 3rd instar larval gut tissue and eye disc were done to examine the in-vivo **KBH** interaction with  $\text{Cu}^{2+}$ . The capability of **KBH** for the early diagnosis of  $\text{Cu}^{2+}$ - induced amyloid toxicity was investigated in eye imaginal disc of *AD Drosophila* 3rd instar larvae.

**Table 2**

Comparison table of previous reports on colorimetric  $\text{Cu}^{2+}$  sensing.

S. No.	Chemosensor	Solvent	LOD ( $\text{M}^{-1}$ )	Reversibility	Application	Ref.
1.	Chromone-based	MeCN:H <sub>2</sub> O (9:1)	$4.6 \times 10^{-7}$	EDTA	real water samples	[41]
2.	Carbazol-based	DMF-buffer (1:1)	$2.9 \times 10^{-6}$	EDTA	–	[42]
3.	Pseudo-crown cysteine based	MeCN	$6.6 \times 10^{-6}$	–	–	[43]
4.	Azo-phenol based	EtOH:H <sub>2</sub> O (1:10)	$7.2 \times 10^{-7}$	–	HeLa cells bioimaging	[44]
5.	Squaraine-based	MeCN	$1.8 \times 10^{-7}$	EDTA	–	[45]
6.	Quinaldine-indole based	MeOH:H <sub>2</sub> O (9:1)	$6.3 \times 10^{-7}$	–	real water samples	[46]
7.	2-Naphthaldehyde based	PBS buffer	$1.0 \times 10^{-6}$	–	–	[47]
8.	1H-Perimidine based	MeOH:H <sub>2</sub> O (1:1)	$3.7 \times 10^{-9}$	EDTA	real water samples	[48]
9.	Pyrene-based	H <sub>2</sub> O	$40 \times 10^{-9}$	–	Bio-imaging in <i>Bohonia Nigalandra</i> and <i>Monilia Albicans</i>	[49]
10.	Acylthiosemicarbazide-based	DMSO:H <sub>2</sub> O (9:1)	$1.0 \times 10^{-7}$	–	test strips	[50]
11.	Pyridoxal-based	MeOH:H <sub>2</sub> O (1:1)	$0.14 \times 10^{-6}$	–	–	[51]
12.	Diarylethene-based	H <sub>2</sub> O	$1.5 \times 10^{-9}$	EDTA	AD diagnostic study and bioimaging in <i>Drosophila</i> and real water samples	Our work

## CRedit authorship contribution statement

**Gautam Kumar:** Writing – original draft, Validation, Software, Methodology, Investigation, Formal analysis, Data curation. **Ananya Srivastava:** Writing – original draft, Methodology, Investigation, Data curation. **Prabhat Kumar:** Writing – original draft, Investigation, Data curation. **S. Srikrishna:** Writing – review & editing, Supervision. **Vinod P. Singh:** Writing – review & editing, Supervision, Resources, Funding acquisition, Conceptualization.

## Declaration of competing interest

The authors declare that they have no known competing financial interests or personal relationships that could have appeared to influence the work reported in this paper.

## Acknowledgements

G. Kumar thanks the UGC-New Delhi, India for Junior Research Fellowship [NTA Ref. no. 191620197757]. One of the authors (V.P. Singh) is also thankful to Banaras Hindu University for research grant under IoE Scheme (Dev. Scheme No. 6031).

## Appendix B. Supplementary data

Supplementary data to this article can be found online at <https://doi.org/10.1016/j.heliyon.2024.e24074>.

## References

- [1] J.M. Long, D.M. Holtzman, Alzheimer disease: an update on pathobiology and treatment strategies, *Cell* 179 (2019) 312–339, <https://doi.org/10.1016/j.cell.2019.09.001>.
- [2] D.S. Knopman, H. Amieva, R.C. Petersen, G. Chételat, D.M. Holtzman, B.T. Hyman, et al., Alzheimer disease, *Nat. Rev. Dis. Prim.* 7 (2021) 33, <https://doi.org/10.1038/s41572-021-00269-y>.
- [3] J. Hardy, D.J. Selkoe, The amyloid hypothesis of Alzheimer's disease: progress and problems on the road to therapeutics, *Science* 297 (2002) 353–356, <https://doi.org/10.1126/science.1072994>.
- [4] G.M. Shankar, S. Li, T.H. Mehta, M.A. Garcia, N.E. Shepardson, I. Smith, F.M. Brett, M.A. Farrell, M.J. Rowan, C.A. Lemere, C.M. Regan, D.M. Walsh, B. L. Sabatini, D.J. Selkoe, Amyloid-beta protein dimers isolated directly from Alzheimer's brains impair synaptic plasticity and memory, *Nat. Med.* 14 (2008) 837–842, <https://doi.org/10.1038/nm1782>.
- [5] C.M. Lee, M. Woodward, G.D. Batty, A.S. Beiser, S. Bell, C. Berr, E. Bjertness, J. Chalmers, R. Clarke, J.F. Dartigues, Association of anthropometry and weight change with risk of dementia and its major subtypes: a meta-analysis consisting 2.8 million adults with 57294 cases of dementia, *Obes. Rev.* 21 (2020) e12989, <https://doi.org/10.1111/obr.12989>.
- [6] A.I. Bush, Metal complexing agents as therapies for Alzheimer's disease, *Neurobiol. Aging* 23 (2002) 1031–1038, [https://doi.org/10.1016/S0197-4580\(02\)00120-3](https://doi.org/10.1016/S0197-4580(02)00120-3).
- [7] A.I. Bush, The metallobiology of Alzheimer's disease, *Trends Neurosci.* 26 (2003) 207–214, [https://doi.org/10.1016/S0166-2236\(03\)00067-5](https://doi.org/10.1016/S0166-2236(03)00067-5).
- [8] D. Schenk, R. Barbour, W. Dunn, G. Gordon, H. Grajeda, T. Guido, K. Hu, J. Huang, W.K. Johnson, K. Khan, D. Kholodenko, M. Lee, Z. Liao, I. Lieberburg, R. Motter, L. Mutter, F. Soriano, G. Shopp, N. Vasquez, C. Vandevert, S. Walker, M. Wogulis, T. Yednock, D. Games, P. Seubert, Immunization with amyloid-beta attenuates Alzheimer-disease-like pathology in the PDAPP mouse, *Nature* 400 (1999) 173–177, <https://doi.org/10.1038/22124>.
- [9] G.M. Susanne, W.W. Michael, J.T. Leon, C.P. Ronald, R.J. Clifford, J. William, Q.T. John, W.T. Arthur, B. Laurel, Ways toward an early diagnosis in Alzheimer's disease: the Alzheimer's disease neuroimaging initiative (ADNI), *Alzheimer's Dement.* 1 (2005) 55–66, <https://doi.org/10.1016/j.jalz.2005.06.003>.
- [10] K. Shoghi-Jadid, G.W. Small, E.D. Agdeppa, V. Kepe, L.M. Ercoli, P. Siddarth, S. Read, N. Satyamurthy, A. Petric, S.C. Huang, J.R. Barrio, Localization of neurofibrillary tangles and beta-amyloid plaques in the brains of living patients with Alzheimer disease, *Am. J. Geriatr. Psychiatr.* 10 (2002) 24–35, <https://doi.org/10.1097/00019442-200201000-00004>.
- [11] M.A. Greenough, J. Camakaris, A.I. Bush, Metal dyshomeostasis and oxidative stress in Alzheimer's disease, *Neurochem. Int.* 62 (2013) 540–555, <https://doi.org/10.1016/j.neuint.2012.08.014>.
- [12] J.H. Viles, Metal ions and amyloid fiber formation in neurodegenerative diseases. Copper, zinc and iron in Alzheimer's, Parkinson's and prion diseases, *Coord. Chem. Rev.* 256 (2012) 2271–2284, <https://doi.org/10.1016/j.ccr.2012.05.003>.
- [13] D. Jiang, L. Men, J. Wang, Y. Zhang, S. Chickenyen, Y. Wang, F. Zhou, Redox reactions of copper complexes formed with different  $\beta$ -amyloid peptides and their neuropathological relevance, *Biochemistry* 46 (2007) 9270–9282, <https://doi.org/10.1021/bi700508n>.
- [14] L. Guilloureaux, S. Combalbert, A. Sournia-saquet, H. Mazarguil, P. Fallier, Redox chemistry of copper-amyloid- $\beta$ : the generation of hydroxyl radical in the presence of ascorbate is linked to redox-potentials and aggregation state, *Chembiochem* 8 (2007) 1317–1325, <https://doi.org/10.1002/cbic.200700111>.
- [15] E. Christopher, H. Emily, P. Anthony, M.M. Esiri, Brain burdens of aluminum, iron, and copper and their relationships with amyloid- $\beta$  pathology in 60 human brains, *J. Alzheimers Dis* 31 (2012) 725–730, <https://doi.org/10.3233/JAD-2012-120766>.
- [16] D. Kaden, A.I. Bush, R. Danzeisen, T.A. Bayer, G. Multhaup, Disturbed copper bioavailability in Alzheimer's disease, *Int. J. Alzheimer's Dis.* 2011 (2011) 345614–345619, <https://doi.org/10.4061/2011/345614>.
- [17] L. Pickart, J.M. Vasquez-Soltero, A. Margolina, The effect of the human peptide GHK on gene expression relevant to nervous system function and cognitive decline, *Brain Sci.* 7 (2017) 20–57, <https://doi.org/10.3390/brainsci7020020>.
- [18] D. Jiang, L. Zhang, G.P.G. Grant, C.G. Dudzik, S. Chen, S. Patel, Y. Hao, G.L. Millhauser, F. Zhou, The elevated copper binding strength of amyloid- $\beta$  aggregates allows the sequestration of copper from albumin: a pathway to accumulation of copper in senile plaques, *Biochemistry* 52 (2013) 547–556, <https://doi.org/10.1021/bi301053h>.
- [19] D.P. Smith, D.G. Smith, C.C. Curtain, J.F. Boas, J.R. Pilbrow, G.D. Ciccotosto, T.L. Lau, D.J. Tew, K. Perez, J.D. Wade, A.I. Bush, S.C. Drew, F. Separovic, C. L. Masters, R. Cappai, K.J. Barnham, Copper-mediated amyloid- $\beta$  toxicity is associated with an intermolecular histidine bridge, *J. Biol. Chem.* 281 (2006) 15145–15154, <https://doi.org/10.1074/jbc.M600417200>.
- [20] X. Huang, M.P. Cuajungco, C.S. Atwood, M.A. Hartshorn, J.D.A. Tyndall, G.R. Hanson, K.C. Stokes, M. Leopold, G. Multhaup, L.E. Goldstein, R.C. Scarpa, A. J. Saunders, J. Lim, R.D. Moir, C. Glabe, E.F. Bowden, C.L. Masters, D.P. Fairlie, R.E. Tanzi, A.I. Bush, Cu(II) potentiation of Alzheimer A $\beta$  neurotoxicity:

- Correlation with cell-free hydrogen peroxide production and metal reduction, *J. Biol. Chem.* 274 (1999) 37111–37116, <https://doi.org/10.1074/jbc.274.52.37111>.
- [21] R.A. Cherny, C.S. Atwood, M.E. Xilinas, D.N. Gray, W.D. Jones, C.A. McLean, K.J. Barnham, I. Volitakis, F.W. Fraser, Y.S. Kim, X. Huang, L.E. Goldstein, R. D. Moir, J.T. Lim, K. Beyreuther, H. Zheng, R.E. Tanzi, C.L. Masters, A.I. Bush, Treatment with a copper-zinc chelator markedly and rapidly inhibits beta-amyloid accumulation in Alzheimer's disease transgenic mice, *Neuron* 30 (2001) 665–676, [https://doi.org/10.1016/S0896-6273\(01\)00317-8](https://doi.org/10.1016/S0896-6273(01)00317-8).
- [22] K.D. Fasae, A.O. Abolaji, T.R. Faloye, A.Y. Odunsi, B.O. Oyetayo, J.I. Enya, J.A. Rotimi, R.O. Akinyemi, A.J. Whitworth, M. Aschner, Metallobiology and therapeutic chelation of biomaterials (copper, zinc and iron) in Alzheimer's disease: limitations, and current and future perspectives, *J. Trace Elem. Med. Biol.* 67 (2021) 126779–126800, <https://doi.org/10.1016/j.jtemb.2021.126779>.
- [23] Y. Wang, B. Tang, S. Zhang, A visible colorimetric pH sensitive chemosensor based on azo dye of benzophenone, *Dyes Pigments* 91 (2011) 294–297, <https://doi.org/10.1016/j.dyepig.2011.03.003>.
- [24] B. Naskar, R. Modak, Y. Sikdar, D.K. Maiti, A. Bauzá, A. Frontera, A. Katarkar, K. Chaudhuri, S. Goswami, Fluorescent sensing of Al<sup>3+</sup> by benzophenone based Schiff base chemosensor and live cell imaging applications: impact of keto-enol tautomerism, *Sens. Actuators B: Chem.* 239 (2017) 1194–1204, <https://doi.org/10.1016/j.snb.2016.08.148>.
- [25] C.I. David, N. Bhuvanesh, H. Jayaraj, A. Thamilselvan, D. Parimaladevi, A. Abiram, J. Prabhu, R. Nandhakumar, Experimental and theoretical studies on a simple S–S-bridged dimeric Schiff Base: selective chromo-fluorogenic chemosensor for nanomolar detection of Fe<sup>2+</sup> & Al<sup>3+</sup> ions and its varied applications, *ACS Omega* 5 (2020) 3055–3072, <https://doi.org/10.1021/acsomega.9b04294>.
- [26] A. Kumar, Virender, M. Saini, B. Mohan, Shayloraj, M. Kamboj, Colorimetric and fluorescent Schiff base sensors for trace detection of pollutants and biologically significant cations: a review (2010–2021), *Microchem. J.* 181 (2022) 107798, <https://doi.org/10.1016/j.microc.2022.107798>.
- [27] H.F. Xie, C.J. Yu, Y.L. Huang, H. Xu, Q.L. Zhang, X.H. Sun, X. Feng, C. Redshaw, A turn-off fluorescent probe for the detection of Cu<sup>2+</sup> based on a tetraphenylethylene-functionalized salicylaldehyde Schiff-base, *Mater. Chem. Front.* 4 (2020) 1500–1506, <https://doi.org/10.1039/c9qm00759h>.
- [28] M. Shellaiah, P. Venkatesan, N. Thirumalaivasan, S.P. Wu, K.W. Sun, Pyrene-based fluorescent probe for “Off-on-Off” sequential detection of Cu<sup>2+</sup> and CN<sup>-</sup> with HeLa cells imaging, *Chemosens* 11 (2023) 115–131, <https://doi.org/10.3390/chemosens11020115>.
- [29] F. Ghasemi, M.R. Hormozi-Nezhad, M. Mahmoudi, Label-free detection of  $\beta$ -amyloid peptides (A $\beta$ 40 and A $\beta$ 42): a colorimetric sensor array for plasma monitoring of Alzheimer's disease, *Nanoscale* 10 (2018) 6361–6368, <https://doi.org/10.1039/c8nr00195b>.
- [30] S. Hu, C. Yang, Y. Li, Q. Luo, H. Luo, Nanozymesensor array based on manganese dioxide for the distinction between multiple amyloid  $\beta$  peptides and their dynamic aggregation process, *Biosens. Bioelectron.* 199 (2022) 113881, <https://doi.org/10.1016/j.bios.2021.113881>.
- [31] G. Kumar, A. Srivastava, V.P. Singh, Graphene oxide-supported nickel(II) complex as a reusable nano catalyst for the synthesis of bis (indolyl)methanes, *Dalton Trans.* 52 (2023) 3431–3437, <https://doi.org/10.1039/D2DT04176F>.
- [32] A.K. Manna, J. Mondal, K. Rout, G.K. Patra, A new ICT based Schiff-base chemosensor for colorimetric selective detection of copper and its copper complex for both colorimetric and fluorometric detection of Cysteine, *J. Photochem. Photobiol., A: Chem* 367 (2018) 74–82, <https://doi.org/10.1016/j.jphotochem.2018.08.018>.
- [33] Y.J. Na, Y.W. Choi, J.Y. Yun, K.M. Park, P.S. Chang, C. Kim, Dual-channel detection of Cu<sup>2+</sup> and F<sup>-</sup> with a simple Schiff-based colorimetric and fluorescent sensor, *Spectrochim. Acta Mol. Biomol. Spectrosc.* 136 (2015) 1649–1657, <https://doi.org/10.1016/j.saa.2014.10.060>.
- [34] G. Kumar, A. Srivastava, S. Gond, P. Yadav, A. Singh, V.P. Singh, A reversible and selective chromogenic thiazole tagged chemosensor for Hg<sup>2+</sup> in aqueous medium: crystal structure, theoretical investigations and real sample analysis, *J. Mol. Struct.* 1283 (2023) 135281–135292, <https://doi.org/10.1016/j.molstruc.2023.135281>.
- [35] G. Kumar, A. Srivastava, P. Kumar, S. Srikrishna, V.P. Singh, Fluorescent turn-on anthracene-based aluminium(III) sensor for therapeutic study in Alzheimer's disease model of *Drosophila*, *ACS Chem. Neurosci.* 14 (2023) 2792–2801, <https://doi.org/10.1021/acscchemneuro.3c00340>.
- [36] A. Kumar, B. Purohit, K. Mahato, S. Roy, A. Srivastava, P. Chandra, Design and development of ultrafast synaptic acid sensor, based on electrochemically nanotuned gold nanoparticles and solvothermally reduced graphene oxide, *Electroanalysis* 31 (2019) 59–69, <https://doi.org/10.1002/elan.201900>.
- [37] U.B. Pandey, C.D. Nichols, Human disease models in *Drosophila melanogaster* and the role of the fly in therapeutic drug discovery, *Pharmacol. Rev.* 63 (2011) 411–436, <https://doi.org/10.1124/pr.110.003293>.
- [38] M.F. Pinter, S. Stempler, S.T. Mazaki, Y. Losev, A. Singh-Anand, D.E. Álvarez, J. Lezmy, E. Gazit, E. Ruppín, D. Segal, Altered protein glycosylation predicts Alzheimer's disease and modulates its pathology in disease model *Drosophila*, *Neurobiol. Aging* 56 (2017) 159–171, <https://doi.org/10.1016/j.neurobiolaging.2017.04.020>.
- [39] B.S. Chauhan, A. Rai, A.K. Sonkar, K. Tripathi, S. Upadhyay, L. Mishra, S. Srikrishna, Neuroprotective activity of a novel synthetic rhodamine-based hydrazone against Cu<sup>2+</sup> induced Alzheimer's disease in *Drosophila*, *ACS Chem. Neurosci.* 13 (2022) 1566–1579, <https://doi.org/10.1021/acscchemneuro.2c00144>.
- [40] S. Bagheri, R. Squitti, T. Haertlé, M. Siotto, A.A. Saboury, Role of copper in the onset of Alzheimer's disease compared to other metals, *Front. Aging Neurosci.* 9 (2018) 446–461, <https://doi.org/10.3389/fnagi.2017.00446>.
- [41] G.J. Park, G.R. You, Y.W. Choi, C. Kim, A naked-eye chemosensor for simultaneous detection of iron and copper ions and its copper complex for colorimetric/fluorescent sensing of cyanide, *Sensor. Actuator. B Chem.* 229 (2016) 257–271, <https://doi.org/10.1016/j.snb.2016.01.133>.
- [42] R. Chandra, A. Ghorai, G.K. Patra, A simple benzildihydrazone derived colorimetric and fluorescent ‘on-off-on’ sensor for sequential detection of copper(II) and cyanide ions in aqueous solution, *Sensor. Actuator. B Chem.* 255 (2018) 701–711, <https://doi.org/10.1016/j.snb.2017.08.067>.
- [43] N.A. Morais, L. Fernandes, J.A. Machado, J.L. Capelo, C. Lodeiro, E. Oliveira, An unusual emissive and colorimetric copper (II) detection by a selective probe based on a pseudo-crown cysteine dye: solution and gas phase studies, *Inorg. Chem. Commun.* 86 (2017) 299–303, <https://doi.org/10.1016/j.inoche.2017.11.001>.
- [44] Y. Li, X. Han, Y. Song, An azo-phenol derivative probe: colorimetric and “turn-on” fluorescent detection of copper(II) ions and pH value in aqueous solution, *RSC Adv.* 7 (2017) 20537–20541, <https://doi.org/10.1039/C7RA01109A>.
- [45] Y. Liu, L. Wang, C. Guo, Y. Hou, A colorimetric squaraine-based probe and test paper for rapid naked eyes detection of copper ion (II), *Tetrahedron Lett.* 59 (2018) 3930–3933, <https://doi.org/10.1016/j.tetlet.2018.09.042>.
- [46] H.S. Kumbhar, B.L. Gadilohar, G.S. Shankarling, A highly selective quinaldine-indole based spiropyran with intramolecular H-bonding for visual detection of Cu (II) ions, *Sensor. Actuator. B Chem.* 222 (2016) 35–42, <https://doi.org/10.1016/j.snb.2015.08.025>.
- [47] Z.Q. Guo, W.Q. Chen, X.M. Duan, Highly selective visual detection of Cu(II) utilizing intramolecular hydrogen bond-stabilized merocyanine in aqueous buffer solution, *Org. Lett.* 12 (2010) 2202–2205, <https://doi.org/10.1021/ol100381g>.
- [48] D.J. Fanna, L.M.P. Lima, A.R. Craze, A. Trinchi, R. Wührer, L.F. Lindoy, G. Wei, J.K. Reynolds, F. Li, Ultrasensitive colorimetric and ratiometric detection of Cu<sup>2+</sup>: acid-base properties, complexation, and binding studies, *ACS Omega* 3 (2018) 10471–10480, <https://doi.org/10.1021/acsomega.8b01483>.
- [49] S. Paul, P. Ghosh, S. Bhuyan, S.K. Mukhopadhyay, P. Banerjee, Nanomolar level selective dual channel sensing of Cu<sup>2+</sup> and CN<sup>-</sup> from aqueous medium by an opto-electronic chemoreceptor, *Dalton Trans.* 47 (2018) 1082–1091, <https://doi.org/10.1039/C7DT03802J>.
- [50] Q. Lin, P. Chen, J. Liu, Y.P. Fu, Y.M. Zhang, T.B. Wei, Colorimetric chemosensor and test kit for detection copper(II) cations in aqueous solution with specific selectivity and high sensitivity, *Dyes Pigments* 98 (2013) 100–105, <https://doi.org/10.1016/j.dyepig.2013.01.024>.
- [51] L. Qu, C. Yin, F. Huo, J. Chao, Y. Zhang, F. Cheng, A pyridoxal-based dual chemosensor for visual detection of copper ion and ratiometric fluorescent detection of zinc ion, *Sensor. Actuator. B Chem.* 191 (2014) 158–164, <https://doi.org/10.1016/j.snb.2013.09.114>.